

# Diabological touching point in the magnetic energy levels of topological nodal-line metals

Chong Wang,<sup>1</sup> Zhongyi Zhang,<sup>2</sup> Chen Fang,<sup>2,\*</sup> and A. Alexandradinata<sup>3,†</sup>

<sup>1</sup>Department of Physics, Carnegie Mellon University, Pittsburgh, Pennsylvania 15213, USA

<sup>2</sup>Institute of Physics, Chinese Academy of Sciences, Beijing 100080, China

<sup>3</sup>Department of Physics and Institute for Condensed Matter Theory,

University of Illinois at Urbana-Champaign, Urbana, Illinois 61801, USA

(Dated: October 5, 2020)

For three-dimensional metals, Landau levels disperse as a function of the magnetic field and the momentum wavenumber parallel to the field. In this two-dimensional parameter space, it is shown that two conically-dispersing Landau levels can touch at a diabological point – a *Landau-Dirac point*. The conditions giving rise to Landau-Dirac points are shown to be magnetic breakdown (field-induced quantum tunneling) and certain crystallographic spacetime symmetry. Both conditions are realizable in topological nodal-line metals, as we exemplify with  $\text{CaP}_3$ . A Landau-Dirac point reveals itself in anomalous “batman”-like peaks in the magnetoresistance, as well as in the onset of optical absorption linearly evolving to zero frequency as a function of the field magnitude/orientation.

For a real Hamiltonian, energy-level surfaces over a two-dimensional parameter space can locally form a double cone (*diabolo*) with an energy-degenerate vertex known as a *diabological point* [1–4]. The first physical application of the diabological point was by W. R. Hamilton in his 1832 prediction of conical refraction [5, 6]. Since then, the diabological point has re-emerged in diverse phenomena in singular optics [7], nuclear [8–11] and quantum [12] physics. Its most recent revival is as Dirac-Weyl points [13] in the crystal-momentum space of topological semimetals [14–18] and insulators [19–22].

This work presents a heretofore undiscovered type of diabological point in a textbook solid-state phenomenon: the quantized energy spectrum of three-dimensional metals subject to a homogeneous magnetic field. A fundamental feature of the magnetic energy spectrum is its quantization into Landau levels [23], which are naturally parametrized by the field ( $B$ ) and the momentum wavenumber ( $k_z$ ) parallel to the field. In this two-dimensional parameter space, Fig. 1(b) illustrates how two Landau-level surfaces can touch at a diabological point, which in the magnetic context will be referred to as a *Landau-Dirac point*. Parallel transport around an equienergy contour of the Landau-Dirac cone gives a  $\pi$  Berry phase [24] which is topologically quantized.

Landau-Dirac points do *not* exist for the free electron gas, nor do they exist for conventional metals with parabolic energy bands. To appreciate this, consider that the Landau levels (in both cases) are determined by the Onsager-Lifshitz-Roth quantization rule [25–27]:  $\hbar/eB = (2\pi n + \gamma)/S(E, k_z)$ , which is universally valid for weak fields.  $S(E, k_z)$  is the  $k$ -area enclosed by the orbit,  $0 \leq n \in \mathbb{Z}$  is the Landau-level index, and  $\gamma$  is a subleading-in- $B$  correction inclusive of the Maslov [28] and Berry phases [27, 29], and a dynamical phase originating from the generalized Zeeman interaction [27, 30]. Henceforth, we set  $\hbar=e=1$  so that  $B^{-1}$  equals the square of the magnetic length. Generally for an electron-like (resp. hole-like) pocket,  $S(E, k_z)$  is a single-valued function of  $k_z$  and an increasing (resp. decreasing) function of energy  $E$ , e.g.,  $S = \pi(2mE - k_z^2)$  for a free-electron gas with mass  $m$ . These conditions on  $S(E, k_z)$  ensure that equienergy solutions of the quantization

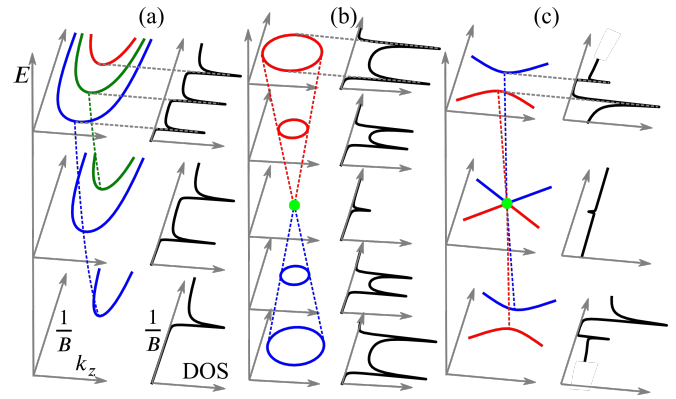


FIG. 1. Magnetic energy levels for a free-electron gas (a), and for topological nodal-line metals (b-c). Left of each panel: equienergy contours of energy-level surfaces in  $(B^{-1}, k_z)$ -space, with distinct sheets distinguished by color; right: corresponding density of states, regularized by a finite lifetime.

rule lie on *open*, non-intersecting contours in  $(B^{-1}, k_z)$ -space, as illustrated for the free-electron gas in Fig. 1(a). It follows that the *closed* equienergy contours of the diabolo [cf. Fig. 1(b)] cannot derive from a single electron-like or hole-like pocket.

However, if multiple pockets are linked by field-driven quantum tunneling (known as magnetic breakdown [31–35]), we will show that tunneling-induced level repulsion can convert open contours to closed contours of a diabolo. The stability of the Landau-Dirac point relies on a certain crystallographic spacetime symmetry that is preserved in the presence of the field. For example, the composition  $Tc_{2y}$  of time reversal and two-fold rotation (about a field-orthogonal axis) maps  $(B^{-1}, k_z) \rightarrow (B^{-1}, k_z)$ , ensuring that Landau-Dirac points are movable over  $(B^{-1}, k_z)$ -space, but irremovable unless annihilated in pairs – as analogous to the Dirac points of graphene [15]. Either of spatial inversion  $\mathbf{i}$  [ $(x, y, z) \rightarrow (-x, -y, -z)$ ] or reflection  $\mathbf{r}_z$  [ $(x, y, z) \rightarrow (x, y, -z)$ ] maps  $(B^{-1}, k_z) \rightarrow (B^{-1}, -k_z)$ , and therefore crossings between Landau levels of opposite  $\mathbf{i}$  (or  $\mathbf{r}_z$ ) representations are perturbatively robust on high-symmetry lines. All three symmetries,

as well as the condition of magnetic breakdown, are realizable in topological nodal-line metals [36–41] – as we will first demonstrate with a conceptually-simple, minimal model, and subsequently for the nodal-line metallic candidate  $\text{CaP}_3$ . We will show further that a Landau-Dirac point reveals itself in anomalous “batman”-like peaks in the density of states [cf. Fig. 1(b)], which leaves an experimental fingerprint in the magnetoresistance as well as in optical absorption.

*Proof of principle.* We first present a minimal model of Landau-Dirac points with both  $\mathbf{r}_z$  and  $Tc_{2y}$  symmetries. At zero field, our effective-mass model describes two parabolic bands with opposite masses:

$$H(\mathbf{k}) = \left[ (k_x^2 + k_y^2)/2m - \epsilon_0 \right] \tau_3 + v_z k_z \tau_1 + v_x k_x. \quad (1)$$

$\epsilon_0$  being positive implies that the two bands overlap on the energy axis, however level repulsion is absent in the  $k_z=0$  plane owing to  $\mathbf{r}_z$  symmetry:  $\tau_3 H(\mathbf{k}) \tau_3 = H(k_x, k_y, -k_z)$ . It follows that a zero-energy, nodal-line degeneracy encircles  $\mathbf{k}=\mathbf{0}$  with radius  $k_R = \sqrt{2m\epsilon_0}$ , supposing  $v_x=0$ . If nonzero, the  $v_x k_x$  term causes the nodal line to disperse with bandwidth  $\Delta E = 2v_x k_R$ . Thus for a Fermi energy satisfying  $|E_F| < \Delta E/2$ , the Fermi surface comprises electron and hole pockets that interconnect like a linked sausage, as illustrated in Fig. 2(b). Close to either interconnection points (with  $E_F=0$ ), an effective Hamiltonian is attained by linearizing Eq. (1) around  $\mathbf{k}=(0, \pm k_R, 0)$ :

$$H_{\pm} = \pm v_y \delta k_y \tau_3 + v_z k_z \tau_1 + v_x k_x, \quad v_y = \sqrt{2\epsilon_0/m}. \quad (2)$$

whose equienergy contours form a hyperbola depicted in the inset of Fig. 2(a).

Applying a magnetic field parallel to  $-z$ , the magnetic energy levels are eigenvalues of the Peierls-Onsager Hamiltonian  $H(K_x, K_y, k_z)$ , which is obtained by the standard substitution of  $(k_x, k_y)$  in the zero-field Hamiltonian [cf. Eq. (1)] by non-commuting operators satisfying  $[K_y, K_x] = iB$  [42, 43]. If  $B$  is much smaller than the  $\mathbf{k}$ -area of both sausage-shaped pockets, the following semiclassical interpretation holds: the Lorentz force pushes electrons along semiclassical trajectories indicated by arrows in Fig. 2(a). In the vicinity of both connection points [ $\mathbf{k}=(0, \pm k_R, 0)$ ], inter-pocket tunneling occurs with the Landau-Zener probability [33, 44]:

$$\rho^2 = e^{-2\pi\mu}, \quad \mu = S_{\square}/8B, \quad S_{\square} = 4v_z^2 k_z^2 / v_x v_y, \quad (3)$$

with  $S_{\square}$  the rectangular area inscribed by the two hyperbolic arms [cf. inset of Fig. 2(a)]. An analogous type of interband magnetic breakdown was first studied by Slutskin [45, 46], and developed by other authors in the context of Dirac-Weyl metals [47–51]. By matching the WKB wave functions [52] at the tunneling regions (by the Landau-Zener connection formula [49]), we arrive at the following quantization rule for the magnetic energy levels:

$$0 = Q(E, k_z, B^{-1}) = \cos X + \rho^2 \cos Y + \tau^2 \cos Z, \quad (4)$$

$$(X, Y, Z) = \frac{1}{2B} (S_1 - S_3, S_{12} + S_{23}, S_1 + S_3 + 4\omega B),$$

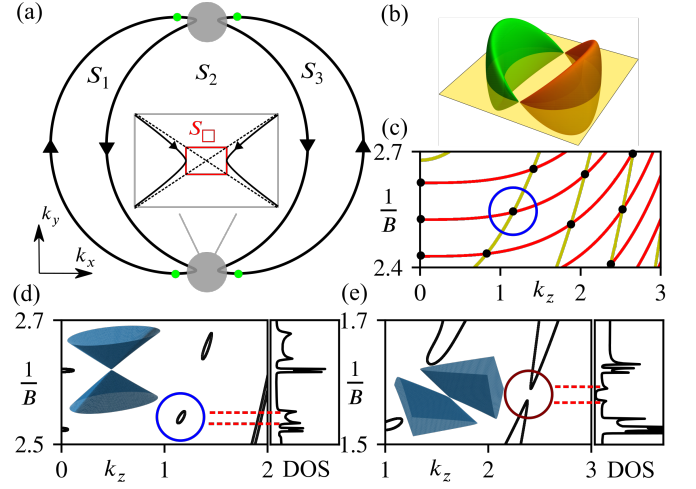


FIG. 2. For the minimal model in Eq. (1) with parameters:  $v_x = v_z = m = 1$  and  $\epsilon_0 = 10$ , we plot the zero-energy, Fermi surface within the Brillouin zone in panel (b); a constant- $(k_z=0.4)$  cross-section of the same surface is shown in (a). Inset of (a): enlarged view of breakdown region. Landau-Fermi surfaces over  $(B^{-1}, k_z)$  are indicated by black dots and black lines in (c,d,e), for  $E=0, 0.01, 0.95$  respectively. Right panels in (d,e) plot the corresponding DOS in arbitrary units. The diablo in (d) [(e)] is the energy dispersion of the type-I (resp., type-II) Landau-Dirac cone encircled in blue (resp., brown).

with  $\tau^2 = 1 - \rho^2$  the probability that an incoming electron ‘reflects’ off the tunneling region with a different velocity.  $\omega = \mu - \mu \ln \mu + \arg[\Gamma(i\mu)] + \pi/4$  is the phase acquired during this adiabatic reflection, with  $\Gamma$  being the Gamma function;  $S_1$  ( $S_3$ ) is the  $\mathbf{k}$ -area of the left (right) sausage-shaped pocket, and  $S_{12} := S_1 + S_2$  ( $S_{23} := S_2 + S_3$ ) is the area of the left (right) circular trajectory linked by tunneling [cf. Fig. 2(a)].

For  $k_z = \mu = 0$ , Landau-Zener tunneling occurs with unit probability, and the solutions to Eq. (4) describe independent cyclotron orbits over overlapping circles:

$$\cos X + \cos Y = 0 \Rightarrow S_{12,23}(E, 0)/B = 2\pi(n + 1/2). \quad (5)$$

The zero-energy solutions of Eq. (5) are doubly-degenerate and lie at equidistant points on the vertical axis of Fig. 2(c), owing to the commensuration of areas:  $S_{12}(0, k_z) = S_{23}(0, k_z)$ , which derives from the effective-mass Hamiltonian in Eq. (1).

There is no unique semiclassical trajectory in the intermediate tunneling regime with nonzero but finite  $\mu \propto k_z^2$ . We focus on a class of solutions contained in certain hypersurfaces in  $(E, k_z, B^{-1})$ -space ( $r$ -space, in short), defined by  $X(r)/\pi \in 2\mathbb{Z}$  and  $2\mathbb{Z} + 1$ . Whether even or odd,  $\cos X$  is extremized to  $\pm 1$ , hence the *only* solutions to Eq. (4) must satisfy  $\cos Y = \cos Z = \mp \cos X$ . These being two constraints within a two-dimensional hypersurface, they can only be satisfied at isolated points which we denote by  $\{\bar{r}\}$ . Such points contained within the  $(X=0)$  hypersurface are illustrated as black dots in Fig. 2(c); note the  $(X=0)$  hypersurface is just the  $E=0$  plane owing to the just-mentioned commensuration condition, and the black dots lie at the intersections of red lines (defined by  $\cos Y = -1$ ) and yellow lines ( $\cos Z = -1$ ).

As we move off a hypersurface in normal (or anti-normal)

direction, each point solution evolves into an elliptical closed curve, as illustrated for  $E=0.01$  in Fig. 2(d). To demonstrate generally that  $\bar{r}$  is a diabolical point, consider that  $\bar{r}$  is an extremal point for each of  $\{\cos X, \cos Y, \cos Z\}$ . Consequently, for any solution of the quantization rule that deviates from  $\bar{r}$  by small  $\delta r = (\delta E, \delta k_z, \delta B^{-1})$ ,  $0 = Q(\bar{r} + \delta r) - Q(\bar{r})$  must be satisfied, with the right-hand side being quadratic in  $\delta r$  to the lowest order. Solving this quadratic equation for the Landau-level dispersion,

$$\begin{aligned} \delta E &= \left(-b \pm \sqrt{b^2 - 4ac}\right) / 2a, \quad a = X_E^2 - \rho^2 Y_E^2 - \tau^2 Z_E^2, \\ b &= [2X_E(\delta k_z X_z + \delta B^{-1} X_{B^{-1}})] - \rho^2[X \rightarrow Y] - \tau^2[X \rightarrow Z], \\ c &= [(\delta k_z X_z + \delta B^{-1} X_{B^{-1}})^2] - \rho^2[X \rightarrow Y] - \tau^2[X \rightarrow Z]. \end{aligned}$$

$X_{E,z,B^{-1}}$  denotes the partial derivative of  $X$  with respect to  $(E, k_z, B^{-1})$ , as evaluated at  $\bar{r}$ ;  $[X \rightarrow Y]$  denotes the substitution of  $X$  with  $Y$  in the square-bracketed expression on the same line. Since the quantity under the square root is quadratic in  $(\delta k_z, \delta B^{-1})$ , the solution in  $(\delta k_z, \delta B^{-1})$ -space generically forms a diabolo with vertex at  $\bar{r}$ .

The perturbative stability of Landau-Dirac points is guaranteed by  $Tc_2y$  symmetry, which constrains the Peierls-Onsager Hamiltonian as  $H(K_x, K_y, k_z) = H(K_x, -K_y, k_z)$ . Given this anti-unitary constraint, a standard generalization [53] of the von Neumann-Wigner theorem [1] states that the codimension of an eigenvalue degeneracy is two, implying degeneracies are perturbatively stable in a two-dimensional parameter space – given here by  $(B^{-1}, k_z)$ . The Landau-Dirac points at  $k_z=0$  are doubly protected by  $\mathbf{r}_z$  symmetry, because each such point is a crossing between levels in distinct eigenspaces of  $\tau_3$  (the matrix representation of  $\mathbf{r}_z$ ).

*Type-II Landau-Dirac points.* While the  $(X=0)$  hypersurface is simply the  $E=0$  plane,  $(X=\pi j)$  hypersurfaces are increasingly dispersive for larger  $|j|$ . With sufficient dispersion, the conical axis tilts so far from the energy axis, that the diabolo [centered at  $(\bar{E}, \bar{k}_z, \bar{B}^{-1})$ ] intersects the  $E=\bar{E}$  plane on open lines; such a *type-II Landau-Dirac point* occurs if and only if  $ac < 0$  on any segment of a circle encircling the diabolical point. A type-II point lying on the  $X=6\pi$  hypersurface is illustrated in Fig. 2(e).

An isolated, type-I point is distinguishable from type-II by the Fermi-level density of states (DOS). The intersection of a Landau-Dirac diabolo with the Fermi level defines a *Landau-Fermi surface* parametrized by a multi-valued function  $B^{-1}(k_z)$  with two extrema, where the DOS diverges as two van-Hove singularities. The DOS in the vicinity of a single van-Hove peak is left-right asymmetric, being proportional to  $[\pm(B^{-1} - B_0^{-1})]^{-1/2}$  on one side but not the other. (Such left-right asymmetry is routinely measured in thermodynamic/galvanomagnetic experiments on analogous solid-state systems [54–56].) Fig. 1 illustrates that the inverse-square-root ‘tails’ (in a type-I scenario) trail toward each other, resembling the helm of Batman; conversely, type-II tails trail apart, like anti-Batman.

*Sum-over-histories approach to DOS.* The existence of

(anti-)Batman peaks can be confirmed by computing the DOS from our quantization rule in Eq. (4). We offer an alternative method of computation that is not only numerically efficient, but also instructively interprets the DOS – as a sum of probability amplitudes for all possible closed-loop Feynman trajectories in  $(k_x, k_y)$ -space. Such trajectories are naturally described in the language of graphs [49]: the equienergy contours of any band structure correspond to a graph with edges oriented by the Lorentz force; distinct edges are connected by two-in-two-out nodes, where interband tunneling or adiabatic reflection occurs. Fig. 2(a) shows that the graph of our model has four edges (labelled  $\alpha=1 \dots 4$ ) connected by two nodes (indicated by grey circles).

A Feynman trajectory  $\lambda$ , defined as an ordered set of connected edges and nodes, is traversed with probability amplitude  $A_\lambda e^{i\phi_\lambda}$ ;  $A_\lambda \in \mathbb{R}$  is a product of  $\tau$  (one power for each reflection) and  $\rho$  (one for each tunneling). The phase  $\phi_\lambda$  sums contributions from edges and nodes: (a) an electron traversing an edge  $\alpha \in \lambda$  [given by  $k_x = k_x^\alpha(k_y)$ ] acquires a phase  $\varphi_\alpha = \int -k_x^\alpha dk_y / B + g_\alpha + m_\alpha \pi / 2$ , with the first term being the dynamical phase [25, 26], the second the geometric Berry phase [27, 29], and the third the Maslov phase [28] from crossing  $m_\alpha$  number of turning points. (b) An electron crossing a node acquires *either* the phase  $\omega$  ( $-\omega$ ) for adiabatic reflection within the higher-energy (resp. lower-energy) band, *or* a  $\pi$  phase [49] for tunneling from lower- to higher-energy band, *or* a trivial phase for tunneling from higher to lower energy. For example, the net phase acquired around the sausage loop (with area  $S_1$ ) is  $\phi_1 = S_1 / B + 2\omega + \pi$ , with  $2\omega$  associated to two adiabatic reflections, and  $\pi$  associated to two turning points indicated by green dots in Fig. 2(a).

The DOS  $\nu(\epsilon)$ , in units of the extensive Landau-level degeneracy  $\mathcal{D}$ , is expressible as a sum of amplitudes for all possible Feynman loops:

$$\frac{\nu}{\mathcal{D}} = \sum_{k_z} \left| \sum_{\alpha} \frac{\partial_\epsilon \varphi_\alpha}{2\pi} (1 + 2 \operatorname{Re} P_{\alpha\alpha}) \right|, \quad P_{\beta\alpha} = \sum_{\lambda \in L_{\beta\alpha}} A_\lambda e^{i\phi_\lambda}. \quad (6)$$

with  $\operatorname{Re} P = (P + P^*) / 2$ , and  $L_{\alpha\beta}$  defined as the set of all trajectories emerging from the start point of edge  $\alpha$  and converging to the start point of edge  $\beta$ ;  $|\partial_\epsilon \varphi_\alpha|$ , to leading order in  $B^{-1}$ , equals the time taken for an electron to traverse edge  $\alpha$  following the semiclassical equation of motion. The above, formally-divergent formula is regularized by replacing  $\varphi_\beta \rightarrow \varphi_\beta + i0^+$  (for all  $\beta$ ) in  $P[\{\varphi_\beta\}]$ . A similar formula for the DOS was first proposed by Kaganov and Slutskin [46] but contains a minor error that is clarified in the Supplemental Material [57].

To evaluate Eq. (6) efficiently, we exploit that  $P_{\beta\alpha}$  satisfies a set of closed, recursive and linear equations, e.g.,  $P_{11} = \tau e^{i\omega} e^{i\phi_2} P_{21} + \rho e^{i\pi} e^{i\phi_3} P_{31}$  because all paths in  $L_{11}$  must return to the start point of edge 1, either by reflection from edge 2 or by tunneling from edge 3. Each of  $\{P_{\beta\alpha}\}_{\alpha,\beta=1\dots 4}$  satisfies an analogous equation, giving an inhomogeneous system of 16 linear equations with 16 unknowns, whose unique solution gives us the DOS via Eq. (6). We plot  $\rho$  in the right panels of

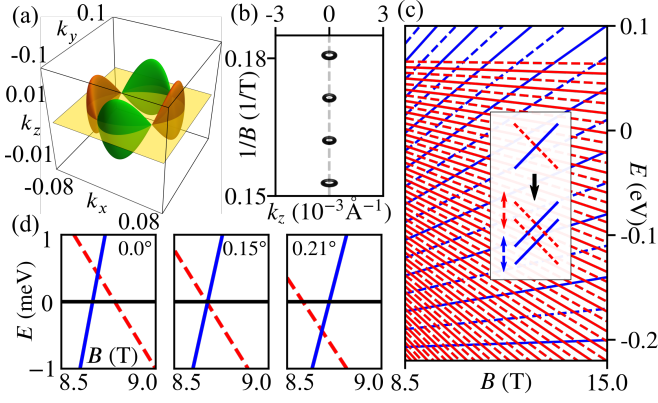


FIG. 3. For  $\text{CaP}_3$  without spin-orbit coupling, we plot (a) the Fermi surface, (b) Landau-Fermi surface, and (c) Landau-level dispersion at  $k_z=0$  and field angle  $\theta_B=0$ . Panel (d) shows the dispersion of a specific Landau-Dirac point at  $\theta_B=0^\circ, 0.15^\circ, 0.21^\circ$ . Inset of (c) schematically illustrates a spin-split Landau-Dirac point.

Fig. 2(d-e), with the correspondence between Batman peaks and type-I Landau-Fermi surfaces (anti-Batman and type-II) indicated by red dashed lines in Fig. 2(d) [resp. Fig. 2(e)].

Our sum-over-histories formula for the Batman peak manifests that it cannot be attributed to a unique semiclassical trajectory in the presence of intermediate tunneling strength. Consequently, Batman peaks are generally non-periodic in  $1/B$  unlike conventional peaks in quantum oscillations; the width of the Batman helm is likewise *not* attributable to the area of any  $\mathbf{k}$ -loop in the graph. With multiple Landau-Dirac points, it is possible that batman and antibatman peaks overlap on the  $B^{-1}$  axis [as is nearly the case in Fig. 2(d)], rendering their experimental identification ambiguous; this ambiguity is reduced by studying the evolution of the DOS as the candidate Landau-Dirac point is brought to the Fermi level, as will be explained near Letter-end.

**$\text{CaP}_3$ .** Our final case study is the time-reversal-invariant, nodal-line metal  $\text{CaP}_3$ , whose order-two point group is generated by spatial inversion  $\mathbf{i}$ . Lacking fermiological studies of  $\text{CaP}_3$ , our case study is based on an ab-initio band-structure calculation by Xu et al [58]. Among topological (semi)metal candidates,  $\text{CaP}_3$ ,  $\text{CaAs}_3$  and  $\text{SrP}_3$  are unique in having a Fermi surface that encloses a single, circular nodal line, with no co-existing Fermi-surface pockets that are topologically trivial [58, 59].  $\text{CaP}_3$ 's nodal line is centered at a inversion-invariant wavevector on the BZ boundary, and encircles an area  $\sim 1/50$  the areal dimension of the BZ – this allows for an accurate description by an effective-mass Hamiltonian  $H(\mathbf{k}) = \sum_{i=0}^3 d_i(\mathbf{k})\tau_i$ , with  $\tau_0$  the identity matrix; the two-by-two matrix structure reflects our (present) ignorance of the weak spin-orbit interaction.

Since the nodal line originates from an inversion of distinct representations of  $\mathbf{i}$ , a basis may be found where  $\mathbf{i}$  constrains the Hamiltonian as  $\tau_3 H(\mathbf{k}) \tau_3 = H(-\mathbf{k})$ ; the composition of time reversal and  $\mathbf{i}$  further constrains  $\tau_3 H(\mathbf{k})^* \tau_3 = H(\mathbf{k})$ , which implies  $d_1=0$ , so that nodal-line energy degeneracies are perturbatively stable by standard codimension arguments [1].

Both symmetry constraints imply  $d_0$  and  $d_3$  are even functions of  $\mathbf{k}$ , while  $d_2 = \mathbf{a} \cdot \mathbf{k} + O(k^3)$  with  $\mathbf{a}$  a real three-vector. It is convenient to perform an  $\text{SO}(3)$   $\mathbf{k}$ -rotation so that  $d_1 = a_z k_z$  (with  $a_z = 5.41 \text{ eV \AA}^{-1}$ ) and  $d_0$  is independent of  $k_x, k_y$ , giving

$$d_0 = -0.074 + 54k_x^2 + 5.2k_y^2 + 8.6k_z^2 - 1.8k_y k_z + 11k_x k_z$$

$$d_3 = -0.14 + 78k_x^2 + 29k_y^2 + 45k_z^2 - 21k_x k_y - 3.8k_y k_z + 16k_x k_z$$

with all quadratic coefficients in units of  $\text{eV \AA}^{-2}$  and determined from ab-initio-fitted  $\mathbf{k} \cdot \mathbf{p}$  parameters; the zero in energy is assumed to be the Fermi level, which we fix by charge neutrality. The resultant Fermi surface consists of four pockets (two electron-like and two hole-like) which connect in the  $k_z=0$  plane, as illustrated in Fig. 3(a).  $[H(k_x, k_y, k_z=0), \tau_3]=0$  reflects a  $U(1) \times U(1)$  symmetry of the effective-mass model which is absent in the lattice model. Note  $H_{11}(k_x, k_y, 0)$  is a parabolic dispersion with effective mass  $m_{11}=0.12$  (in units of the free-electron mass); this parabola overlaps (on the energy axis) with the inverted parabola of  $H_{22}$ , with  $m_{22}=0.31$ .

Applying a field in the  $-z$  direction, both  $\mathbf{i}$  and  $U(1) \times U(1)$  symmetries are retained and constrain the Peierls-Onsager Hamiltonian as  $\tau_3 H(K_x, K_y, k_z) \tau_3 = H(-K_x, -K_y, -k_z)$  and  $[\tau_3, H(K_x, K_y, 0)]=0$ , respectively.  $H_{11}(K_x, K_y, 0)$  equivalently describes a quantum harmonic oscillator [23], while  $H_{22}(K_x, K_y, 0)$  describes an inverted oscillator with a cyclotron frequency that is smaller by the factor  $m_{11}/m_{22}=0.39$ ; both oscillator levels are plotted in Fig. 3(c), with blue (red) lines indicating  $\langle \tau_z \rangle = 1$  ( $\langle \tau_z \rangle = -1$ ). For either oscillator, the  $\mathbf{i}$  eigenvalue alternates between adjacent levels [23], as illustrated by alternating solid ( $\mathbf{i}$ -even) and dashed ( $\mathbf{i}$ -odd) lines. Note that the zeroth level of  $H_{11}$  (bottom-most blue line) is  $\mathbf{i}$ -even, while that of  $H_{22}$  (top-most red line) is  $\mathbf{i}$ -odd, owing to the distinct symmetry representations of basis vectors in the effective-mass Hamiltonian. Half of the Landau-Dirac points in Fig. 3(c) are  $\mathbf{i}$ -protected crossings between solid and dashed lines; the other half are protected by  $U(1) \times U(1)$  symmetry but not by  $\mathbf{i}$ . The corresponding Landau-Fermi surface restricted to  $k_z=0$  comprises a set of points [cf. Fig. 3(b)].

For small  $k_z \neq 0$ , the four sausage links in Fig. 3(a) disconnect; electron dynamics in the vicinity of the four disconnected links is again of the Landau-Zener type, with tunneling probability  $\exp(-2\pi\mu)$ . There is no unique, semiclassical trajectory *except* at  $k_z=0$ , where tunneling occurs with unit probability. The previously-determined, point solutions (at  $k_z=0$ ) extend horizontally to form closed lobes encircling the type-I Landau-Dirac points at  $k_z=0$ , as shown in Fig. 3(b). Just as for the previous, minimal model [cf. Fig. 2(c-d)], we see the formation of closed Landau-Fermi surfaces in the  $(B^{-1}, k_z)$ -region where tunneling is intermediate in strength.

Though our analysis has assumed a specific field orientation, half the crossings in Fig. 3(c) are perturbatively stable against tilting of the field, because  $\mathbf{i}$  symmetry is maintained for any field orientation; the other half that relies on  $U(1) \times U(1)$  symmetry will destabilize.

We have thus far neglected spin in the  $\text{CaP}_3$  study. Accounting for the intrinsic Zeeman and spin-orbit interactions

(which maintain  $\mathbf{i}$  symmetry), each spin-degenerate Landau level generically splits in energy, converting a single, spin-degenerate,  $\mathbf{i}$ -protected Landau-Dirac point into four, spin-nondegenerate,  $\mathbf{i}$ -protected Landau-Dirac points, as illustrated in the inset of Fig. 3(c). An order-of-magnitude estimate for this energy splitting is given by the spin-orbit-induced splitting of the nodal-line degeneracy (at zero field), which ranges from 4 to 32 meV [58].

Landau-Dirac points do not generically occur at the Fermi level. However, by tuning  $B^{-1}$ , the two Landau levels (closest to the Fermi level) can be made to cross; by tuning a second parameter (e.g., the field orientation), such crossing, if  $\mathbf{i}$ - or  $\mathbf{r}_z$ -protected, can be brought to the Fermi level. Fig. 3(d) illustrates a Landau-Dirac point being lowered to the Fermi level by tuning the tilt angle  $\theta_B$  in the  $xz$  plane. This manifests in the onset of optical absorption *linearly* evolving to zero frequency as a function of  $\theta_B$  – a smoking gun for the Landau-Dirac point. Such an optical transition between Landau levels of distinct  $\mathbf{i}$  representations is allowed by the dipole selection rule [60]. Simultaneously, the separation between a pair of (anti-)batman peaks in the DOS would linearly evolve to zero, as illustrated analogously in Fig. 1(b-c).

*Outlook.* We began by presenting Landau-Dirac points in  $(B^{-1}, k_z)$ -space as the natural parameter space motivated by general symmetry considerations; on the other hand, Landau-Dirac points in  $(B^{-1}, \theta_B)$ -space are equally compelling for their experimental tunability. Topological nodal-line metals, including  $\text{CaP}_3$ , provide an experimental platform to make Landau-Dirac points a reality, owing to an interplay of magnetic symmetries and breakdown. Future investigations should determine if a similar Landau-Dirac phenomenology exists for two other topological nodal-line material candidates, which host more complicated Fermi surfaces than the present study: (a)  $\text{SrAs}_3$ , a cousin of  $\text{CaP}_3$  with a similar crystalline structure and an experimentally-evidenced, [61–63] nodal-line degeneracy, and (b) the square-net compound  $\text{ZrSiS}$ , for which breakdown has been experimentally demonstrated [64]. Other platforms for Landau-Dirac points plausibly exist, owing to the diversity of magnetic space groups [65], as well as the qualitatively-distinct forms of breakdown in varied solid-state systems [31–35, 45–50, 66]. It is worth remarking that no symmetry is needed [1] for stable Landau-Dirac points in a three-dimensional parameter space, e.g.,  $(B^{-1}, \theta_B, k_z)$  or  $(B^{-1}, \theta_B, \theta'_B)$ , with  $\theta'_B$  an independent tilt angle.

*Acknowledgments.* We thank Di Xiao and Yang Gao for insightful discussions. C. W. was supported by the Department of Energy, Basic Energy Sciences, Materials Sciences and Engineering Division, Pro-QM EFRC (DE-SC0019443). Z. Z. and C. F. were supported by the Ministry of Science and Technology of China under grant number 2016YFA0302400, National Science Foundation of China under grant number 11674370, and Chinese Academy of Sciences under grant numbers XXH13506-202 and XDB33000000. A. A. was supported by the Gordon and Betty Moore Foundation EPiQS Initiative through Grant No. GBMF4305 at the University of Illinois.

C. W. and Z. Z. contributed equally as co-first authors in this work.

\* cfang@iphy.ac.cn

† aalexan7@illinois.edu

- [1] J. von Neumann and E. Wigner, “On the behavior of eigenvalues in adiabatic processes,” *Phys. Z.* **30**, 467 (1929).
- [2] E. Teller, “The crossing of potential surfaces.” *J. Phys. Chem.* **41**, 109–116 (1937).
- [3] Michael Victor Berry, “Semiclassical mechanics of regular and irregular motion,” in *Les Houches Lecture Series, vol. 36*, edited by R. H. G. Helleman G. Iooss and R. Stora (North-Holland, Amsterdam, 1983) p. 171–271.
- [4] Michael Victor Berry and Mark Wilkinson, “Diabolical points in the spectra of triangles,” *Proc. R. Soc. Lond. A* **392**, 15–43 (1984).
- [5] W.R. Hamilton, “Third supplement to an essay on the theory of systems of rays,” *Trans. R. Irish Acad.* **17**, 1–144 (1837).
- [6] M.V. Berry and M.R. Jeffrey, “Conical diffraction: Hamilton’s diabolical point at the heart of crystal optics,” in *Progress in Optics*, Vol. 50, edited by E. Wolf (Elsevier, Amsterdam, Netherlands, 2007) pp. 13 – 50.
- [7] M. V. Berry and M. R. Dennis, “The optical singularities of birefringent dichroic chiral crystals,” *Proc. R. Soc. Lond. A* **459**, 1261–1292 (2003).
- [8] G. Herzberg and H. C. Longuet-Higgins, “Intersection of potential energy surfaces in polyatomic molecules,” *Discuss. Faraday Soc.* **35**, 77–82 (1963).
- [9] C. Alden Mead and Donald G. Truhlar, “On the determination of born–oppenheimer nuclear motion wave functions including complications due to conical intersections and identical nuclei,” *J. Chem. Phys.* **70**, 2284–2296 (1979).
- [10] Lorenz S. Cederbaum, Ronald S. Friedman, Victor M. Ryaboy, and Nimrod Moiseyev, “Conical intersections and bound molecular states embedded in the continuum,” *Phys. Rev. Lett.* **90**, 013001 (2003).
- [11] A.R. Farhan, L.F. Canto, J.O. Rasmussen, and P. Ring, “Form factors for two-nucleon transfer in the diabolical region of rotating nuclei,” *Nucl. Phys. A* **597**, 387 – 407 (1996).
- [12] Alessandro Ferretti, Alessandro Lami, and Giovanni Villani, “Transition probability due to a conical intersection: On the role of the initial conditions and of the geometric setup of the crossing surfaces,” *The Journal of Chemical Physics* **111**, 916–922 (1999).
- [13] H.B. Nielsen and Masao Ninomiya, “The Adler-Bell-Jackiw anomaly and Weyl fermions in a crystal,” *Phys. Lett. B* **130**, 389 – 396 (1983).
- [14] Petr Hořava, “Stability of fermi surfaces and  $K$  theory,” *Phys. Rev. Lett.* **95**, 016405 (2005).
- [15] K. S. Novoselov, A. K. Geim, S. V. Morozov, D. Jiang, M. I. Katsnelson, I. V. Grigorieva, S. V. Dubonos, and A. A. Firsov, “Two-dimensional gas of massless Dirac fermions in graphene,” *Nature* **438**, 197–200 (2005).
- [16] Xiangang Wan, Ari Turner, Ashvin Vishwanath, and Sergey Y. Savrasov, “Topological semimetal and Fermi-arc surface states in the electronic structure of pyrochlore iridates,” *Phys. Rev. B* **83**, 205101 (2011).
- [17] Gabor B. Halasz and Leon Balents, “Time-reversal invariant realization of the weyl semimetal phase,” *Phys. Rev. B* **85**, 035103 (2012).

- [18] Alexey A Soluyanov, Dominik Gresch, Zhijun Wang, Quan-Sheng Wu, Matthias Troyer, Xi Dai, and B Andrei Bernevig, “Type-II weyl semimetals,” *Nature* **527**, 495–498 (2015).
- [19] C. L. Kane and E. J. Mele, “Quantum spin Hall effect in graphene,” *Phys. Rev. Lett.* **95**, 226801 (2005).
- [20] Liang Fu, C. L. Kane, and E. J. Mele, “Topological insulators in three dimensions,” *Phys. Rev. Lett.* **98**, 106803 (2007).
- [21] J. E. Moore and L. Balents, “Topological invariants of time-reversal-invariant band structures,” *Phys. Rev. B* **75**, 121306 (2007).
- [22] Rahul Roy, “Topological phases and the quantum spin hall effect in three dimensions,” *Phys. Rev. B* **79**, 195322 (2009).
- [23] L. D. Landau and E. M. Lifshitz, *Quantum Mechanics* (Elsevier, Singapore, 2007).
- [24] M. V. Berry, “Quantal phase factors accompanying adiabatic changes,” *Proc. R. Soc. Lond A* **392**, 45 (1984).
- [25] L. Onsager, “Interpretation of the de Haas-van Alphen effect,” *Philos. Mag.* **43**, 1006–1008 (1952).
- [26] L. M. Lifshitz and A.M. Kosevich, “On the theory of the de Haas–van Alphen effect for particles with an arbitrary dispersion law,” *Dokl. Akad. Nauk SSSR* **96**, 963 (1954).
- [27] Laura M. Roth, “Semiclassical theory of magnetic energy levels and magnetic susceptibility of Bloch electrons,” *Phys. Rev.* **145**, 434–448 (1966).
- [28] Joseph B. Keller, “Corrected Bohr-Sommerfeld quantum conditions for nonseparable systems,” *Ann. Phys. (N. Y.)* **4**, 180 – 188 (1958).
- [29] G. P. Mikitik and Yu. V. Sharlai, “Manifestation of Berry’s phase in metal physics,” *Phys. Rev. Lett.* **82**, 2147–2150 (1999).
- [30] Ming-Che Chang and Qian Niu, “Berry phase, hyperorbits, and the Hofstadter spectrum: Semiclassical dynamics in magnetic Bloch bands,” *Phys. Rev. B* **53**, 7010–7023 (1996).
- [31] Morrel H. Cohen and L. M. Falicov, “Magnetic breakdown in crystals,” *Phys. Rev. Lett.* **7**, 231–233 (1961).
- [32] M. Ya. Azbel, “Quasiclassical quantization in the neighborhood of singular classical trajectories,” *J. Exp. Theor. Phys.* **12**, 891 (1961).
- [33] E. I. Blount, “Bloch electrons in a magnetic field,” *Phys. Rev.* **126**, 1636–1653 (1962).
- [34] A. B. Pippard, “Quantization of coupled orbits in metals,” *Proc. R. Soc. Lond. A* **270**, 1–13 (1962).
- [35] W. G. Chambers, “Magnetic breakdown: Effective hamiltonian and de Haas-van Alphen effect,” *Phys. Rev.* **149**, 493–504 (1966).
- [36] A. A. Burkov, M. D. Hook, and Leon Balents, “Topological nodal semimetals,” *Phys. Rev. B* **84**, 235126 (2011).
- [37] Yuanping Chen, Yuee Xie, Shengyuan A. Yang, Hui Pan, Fan Zhang, Marvin L. Cohen, and Shengbai Zhang, “Nanostructured carbon allotropes with Weyl-like loops and points,” *Nano Lett.* **15**, 6974–6978 (2015).
- [38] Tomáš Bzdušek, QuanSheng Wu, Andreas Rüegg, Manfred Sigrist, and Alexey A. Soluyanov, “Nodal-chain metals,” *Nature* **538**, 75–78 (2016).
- [39] Ching-Kai Chiu and Andreas P. Schnyder, “Classification of reflection-symmetry-protected topological semimetals and nodal superconductors,” *Phys. Rev. B* **90**, 205136 (2014).
- [40] Bohm-Jung Yang, Troels Arnfred Bojesen, Takahiro Morimoto, and Akira Furusaki, “Topological semimetals protected by off-centered symmetries in nonsymmorphic crystals,” *Phys. Rev. B* **95**, 075135 (2017).
- [41] Chen Fang, Hongming Weng, Xi Dai, and Zhong Fang, “Topological nodal line semimetals,” *Chin. Phys. B* **25**, 117106 (2016).
- [42] R. Peierls, “Zur theorie des diamagnetismus von leitungsselektronen,” *Z. Phys.* **80**, 763–791 (1933).
- [43] J. M. Luttinger, “The effect of a magnetic field on electrons in a periodic potential,” *Phys. Rev.* **84**, 814–817 (1951).
- [44] Clarence Zener and Ralph Howard Fowler, “Non-adiabatic crossing of energy levels,” *Proc. R. Soc. Lond. A* **137**, 696–702 (1932).
- [45] A.A. Slutskin, “Dynamics of conduction electrons under magnetic breakdown conditions,” *J. Exp. Theor. Phys.* **26**, 474 (1968).
- [46] M.I. Kaganov and A.A. Slutskin, “Coherent magnetic breakdown,” *Phys. Rep.* **98**, 189 – 271 (1983).
- [47] T. E. O’Brien, M. Diez, and C. W. J. Beenakker, “Magnetic breakdown and Klein tunneling in a type-II Weyl semimetal,” *Phys. Rev. Lett.* **116**, 236401 (2016).
- [48] A. Alexandradinata and Leonid Glazman, “Geometric phase and orbital moment in quantization rules for magnetic breakdown,” *Phys. Rev. Lett.* **119**, 256601 (2017).
- [49] A. Alexandradinata and Leonid Glazman, “Semiclassical theory of Landau levels and magnetic breakdown in topological metals,” *Phys. Rev. B* **97**, 144422 (2018).
- [50] Chong Wang, Wenhui Duan, Leonid Glazman, and A. Alexandradinata, “Landau quantization of nearly degenerate bands and full symmetry classification of Landau level crossings,” *Phys. Rev. B* **100**, 014442 (2019).
- [51] M. Breitkreiz, N. Bovenzi, and J. Tworzydło, “Phase shift of cyclotron orbits at type-I and type-II multi-Weyl nodes,” *Phys. Rev. B* **98**, 121403 (2018).
- [52] G.E. Zil’berman, “Theory of Bloch electrons in a magnetic field,” *J. Exp. Theor. Phys.* **5**, 208 (1957).
- [53] A. Alexandradinata and J. Höller, “No-go theorem for topological insulators and high-throughput identification of Chern insulators,” *Phys. Rev. B* **98**, 184305 (2018).
- [54] D. Shoenberg, *Magnetic oscillations in metals* (Cambridge University Press, The Edinburgh Building, Cambridge CB2 8RU, UK, 1984).
- [55] J. S. Dhillon and David Shoenberg, “The de Haas-van Alphen effect III. experiments at fields up to 32KG,” *Philos. Trans. Royal Soc. A* **248**, 1–21 (1955).
- [56] Chunyu Guo, A. Alexandradinata, Carsten Putzke, Feng-Ren Fan, Shengnan Zhang, Quansheng Wu, Oleg V. Yazyev, Kent R. Shirer, Maja D. Bachmann, Eric D. Bauer, Filip Ronning, Claudia Felser, Yan Sun, and Philip J. W. Moll, “Fingerprint of topology in high-temperature quantum oscillations,” (2019), arXiv:1910.07608 [cond-mat.str-el].
- [57] Supplemental Material, which cites Refs. 23, 25, 27–29, 44, 46, 49, 50, 58, 67–70.
- [58] Qiunan Xu, Rui Yu, Zhong Fang, Xi Dai, and Hongming Weng, “Topological nodal line semimetals in the CaP<sub>3</sub> family of materials,” *Phys. Rev. B* **95**, 045136 (2017).
- [59] Y. Quan, Z. P. Yin, and W. E. Pickett, “Single nodal loop of accidental degeneracies in minimal symmetry: Triclinic CaAs<sub>3</sub>,” *Phys. Rev. Lett.* **118**, 176402 (2017).
- [60] Wlodek Zawadzki, “Intraband and interband magneto-optical transitions in semiconductors,” in *Landau level spectroscopy*, edited by G. Landwehr and E. I. Rashba (Elsevier, North-Holland, Amsterdam, 1991) p. 485.
- [61] Shichao Li, Zhaopeng Guo, Dongzhi Fu, Xing-Chen Pan, Jinghui Wang, Kejing Ran, Song Bao, Zhen Ma, Zhengwei Cai, Rui Wang, Rui Yu, Jian Sun, Fengqi Song, and Jinsheng Wen, “Evidence for a Dirac nodal-line semimetal in SrAs<sub>3</sub>,” *Sci. Bull.* **63**, 535 – 541 (2018).
- [62] Linlin An, Xiangde Zhu, Wenshuai Gao, Min Wu, Wei Ning, and Mingliang Tian, “Chiral anomaly and nontrivial Berry phase in the topological nodal-line semimetal SrAs<sub>3</sub>,” *Phys.*

- Rev. B **99**, 045143 (2019).
- [63] M. Mofazzel Hosen, Gyanendra Dhakal, Baokai Wang, Narayan Poudel, Klauss Dimitri, Firoza Kabir, Christopher Sims, Sabin Regmi, Krzysztof Gofryk, Dariusz Kaczorowski, Arun Bansil, and Madhab Neupane, “Experimental observation of drumhead surface states in SrAs<sub>3</sub>,” *Sci. Rep.* **10**, 2776 (2020).
- [64] S. Pezzini, M.R. Van Delft, L.M. Schoop, B.V. Lotsch, A. Carrington, M.I. Katsnelson, N.E. Hussey, and S. Wiedmann, “Unconventional mass enhancement around the Dirac nodal loop in ZrSiS,” *Nat. Phys.* **14**, 178–183 (2018).
- [65] C. J. Bradley and B. L. Davies, “Magnetic groups and their corepresentations,” *Rev. Mod. Phys.* **40**, 359–379 (1968).
- [66] Noah F. Q. Yuan, Hiroki Isobe, and Liang Fu, “Magic of high-order van Hove singularity,” *Nat. Commun.* **10**, 5769 (2019).
- [67] L. M. Lifshitz and A.M. Kosevich, “Theory of magnetic susceptibility in metals at low temperatures,” *J. Exp. Theor. Phys.* **2**, 636 (1956).
- [68] L. M. Falicov and Henryk Stachowiak, “Theory of the de Haas-van Alphen effect in a system of coupled orbits. application to magnesium,” *Phys. Rev.* **147**, 505–515 (1966).
- [69] J. Zak, “Magnetic translation group,” *Phys. Rev.* **134**, A1602–A1606 (1964).
- [70] E. Brown, “Bloch electrons in a uniform magnetic field,” *Phys. Rev.* **133**, A1038–A1044 (1964).

# Supplemental material for ‘Diaboliocal touching point in the magnetic energy levels of topological nodal-line metals’

Chong Wang,<sup>1</sup> Zhongyi Zhang,<sup>2</sup> Chen Fang,<sup>2</sup> and A. Alexandradinata<sup>3</sup>

<sup>1</sup>*Department of Physics, Carnegie Mellon University, Pittsburgh, Pennsylvania 15213, USA*

<sup>2</sup>*Institute of Physics, Chinese Academy of Sciences, Beijing 100080, China*

<sup>3</sup>*Department of Physics and Institute for Condensed Matter Theory, University of Illinois at Urbana-Champaign, Urbana, Illinois 61801, USA*

## CONTENTS

I. Magnetic energy levels of two-pocket model	1
A. Quantization rule	1
B. Density of states	2
II. Additional analysis of CaP <sub>3</sub>	3
A. Effective-mass model of CaP <sub>3</sub>	3
B. Landau levels of CaP <sub>3</sub>	4
References	6

## I. MAGNETIC ENERGY LEVELS OF TWO-POCKET MODEL

For our two-pocket model of a nodal-line metal subject to magnetic breakdown, we offer a more detailed description of the quantization rule [Eq. (4) in main text] and sum-over-histories formula [Eq. (6) in main text] for the density of states (DOS).

### A. Quantization rule

As described in the main text, at fixed wavenumber  $k_z$  and fixed energy  $\varepsilon$ , the model band structure is mapped onto an oriented graph composed of two two-in-two-out vertices and four edges (labelled by  $\alpha = 1 \dots 4$ ). The two vertices are physically associated to focal points of magnetic breakdown. Each edge is oriented according to the Lorentz force under a field in the  $-z$  direction. The orientation allows to uniquely define a start and end point for edges – each edge starts at a vertex and ends at a distinct vertex. We will present a quantization rule for magnetic energy levels that is valid in the regime  $S_{\min}/B \gg 1$ , where  $S_{\min}$  as the area of the smallest loop in the graph (corresponding to one of two sausages).

Let us define  $U_{\beta\alpha}$  as the complex-valued amplitude for an electron to (i) traverse said edge  $\alpha$  and accumulate a phase factor  $\exp(i\varphi_\alpha)$  (to be specified below), and (ii) to subsequently scatter (at a vertex at the end point of  $\alpha$ ) into a possibly-distinct edge  $\beta$  with amplitude  $V_{\beta\alpha}$ . Collecting all 16 elements into a  $4 \times 4$  matrix,  $U$  can be expressed as the product of  $V$  with a diagonal matrix:

$$U(\varepsilon, k_z, B) = \begin{pmatrix} 0 & \tau e^{i\omega} & -\rho & 0 \\ \tau e^{i\omega} & 0 & 0 & -\rho \\ \rho & 0 & 0 & \tau e^{-i\omega} \\ 0 & \rho & \tau e^{-i\omega} & 0 \end{pmatrix} \begin{pmatrix} e^{i\varphi_1} & 0 & 0 & 0 \\ 0 & e^{i\varphi_2} & 0 & 0 \\ 0 & 0 & e^{i\varphi_3} & 0 \\ 0 & 0 & 0 & e^{i\varphi_4} \end{pmatrix}. \quad (1)$$

Let us first describe the diagonal matrix which encodes process (i). The phase accumulated on each edge  $\alpha$  is

$$\varphi_\alpha = -B^{-1} \int_\alpha k_x^\alpha dk_y + m_\alpha \frac{\pi}{2} + \varphi_\alpha^g. \quad (2)$$

The first term is the leading-order dynamical phase<sup>1,2</sup>, with  $k_x = k_x^\alpha(k_y, k_z, \varepsilon)$  defining a  $\mathbf{k}$ -curve corresponding to the edge  $\alpha$ , and the above line integral is oriented by the Lorentz force.  $k_x^{2,3}$  are single-valued functions, however  $k_x^1$  (and also  $k_x^4$ ) is a multivalued function with three branches because edge 1 (resp. edge 4) contains two turning points, where  $\partial k_x^\alpha / \partial k_y = 0$ . The

subleading correction to  $\varphi_\alpha$  sums the Maslov phase<sup>3</sup> ( $\pi/2$  times the number of turning points) and the geometric Berry phase  $\varphi_\alpha^{g,4,5}$ .

Each two-in-two-out vertex is associated to four nonzero amplitudes  $V_{\beta\alpha}$  which can be collected into a two-by-two, unitary ‘scattering matrix’<sup>6</sup>:

$$S(\mu) = \begin{pmatrix} \tau e^{i\omega} & -\rho \\ \rho & \tau e^{-i\omega} \end{pmatrix} \quad (3)$$

with  $\mu = v_z^2 k_z^2 / 2v_x v_y B$ ,  $\rho = \exp(-\pi\mu)$ ,  $\tau = \sqrt{1 - \rho^2}$  and  $\omega = \mu - \mu \ln \mu + \arg[\Gamma(i\mu)] + \pi/4$ .  $|S_{12}|^2 = \exp(-2\pi\mu)$  is identified with the Landau-Zener tunneling probability<sup>7</sup>. For a pair of edges  $(\beta, \alpha)$  that are not connected by a vertex, we define  $V_{\beta\alpha} = 0$ .

The quantization rule determines energy levels by the condition that the four-component wave function (one component for each edge) is single-valued over the graph. This rule is conveniently expressed as<sup>6,8</sup>

$$\det[I - U(E, k_z, B)] = 0, \quad (4)$$

where  $I$  is the  $4 \times 4$  identity matrix. Inserting our expression for  $U$  into Eq. (4) and evaluating the determinant, one obtains the quantization rule for our two-pocket model, as expressed in Eq. (4) of the main text.

## B. Density of states

The density of states (DOS) involves an interference of all possible Feynman loops, even loops that are integer repetitions of a fundamental loop<sup>9</sup>. Let us therefore construct a four-by-four matrix  $P$  from the geometric series:

$$P = \sum_{n=1}^{\infty} U^n, \quad P = UP + U, \quad (5)$$

such that  $P_{\alpha\beta}$  is a sum of amplitudes for trajectories of all possible lengths indexed by  $n$ , where the length of a path is the number of edges traversed. The second equality in Eq. (5) can be viewed element by element as an inhomogeneous system of linear equations for sixteen variables  $P_{\alpha\beta}$ ;  $P = U(1 - U)^{-1}$  is easily calculated once  $U$  is determined from Eq. (1).

The  $P$  matrix is related to the DOS  $\nu$  as

$$\nu(\varepsilon) \approx \frac{D}{2\pi} \left| \sum_{\alpha} (\partial_{\varepsilon} \varphi_{\alpha}) [2 \operatorname{Re}(P_{\alpha\alpha}) + 1] \right|_{\varphi \rightarrow \varphi + i0^+} \quad (6)$$

with a correction of relative magnitude  $|dS_{\square}/dE|/|dS_{\min}/dE|$ ; we remind the reader that  $S_{\square}$  is the area of the  $\mathbf{k}$ -rectangle illustrated in the inset of Fig. 2(a) of the main text.  $D$  above is the degeneracy of a single Landau level. The right-hand side of Eq. (6) depends on the energy  $\varepsilon$  through  $\varphi_{\alpha}$  and the scattering matrix. To make the right-hand side of Eq. (6) well-defined as a generalized function, we replace  $\varphi_{\alpha} \rightarrow \varphi_{\alpha} + i0^+$  for all  $\alpha$ , with  $0^+$  a positive infinitesimal.

In comparison with existing literature, it was proposed by Kaganov and Slutskin [in Ref. 8] that the density of states equals

$$\nu(\varepsilon) \stackrel{?}{=} \frac{D}{2\pi} \sum_{\alpha} \left| (\partial_{\varepsilon} \varphi_{\alpha}) [2 \operatorname{Re}(P_{\alpha\alpha}) + 1] \right|_{\varphi \rightarrow \varphi + i0^+}; \quad (7)$$

$|\partial_{\varepsilon} \varphi_{\alpha}|$ , to leading order in  $B^{-1}$ , equals the time  $T_{\alpha}$  taken for an electron to traverse edge  $\alpha$  following the semiclassical equation of motion. We observe that Eq. (7) differs from our formula [cf. Eq. (6)] in where the absolute value symbol is placed, which affects whether certain amplitudes add constructively or subtract destructively.

Postponing a detailed, analytic proof of our formula to a follow-up publication, we offer here a simple numerical demonstration that the Kaganov-Slutskin formula is incorrect. Figure 1 shows the density of states (normalized by  $D$ ) as a function of energy for several Landau levels. Each Landau level corresponds to a delta-function peak that has been broadened into a Lorentzian-like wave form by a finite lifetime. The specific regularization we choose is  $\varphi_{\alpha} \rightarrow \varphi_{\alpha} + i0.00002\varepsilon_0 T_{\alpha}$ . Being a regularization of a delta function, the integration of the density of states over this Lorentzian should give one (in units of  $D$ ). We find numerically that our formula [Eq. (6)] correctly yields 1.0 while the analogous integral for the Kaganov-Slutskin formula [Eq. (7)] significantly deviates from 1.0.

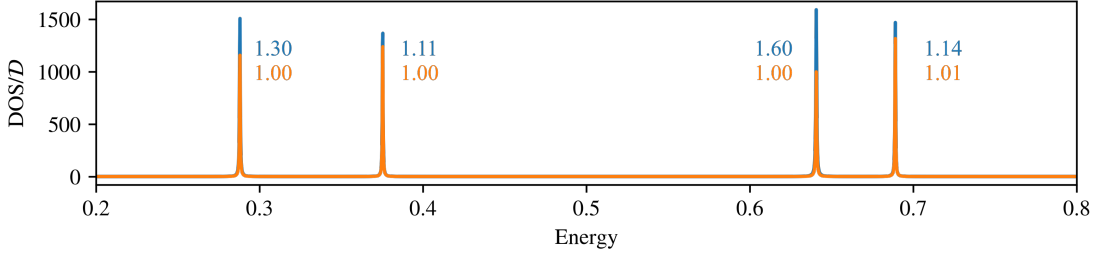


FIG. 1. Density of states calculated by Eq. (7) (resp. blue) and Eq. (6) (resp. yellow) at  $k_z = 2.5$  and  $1/B = 3.0$ . The area under the blue (resp. yellow) line for each peak is annotated beside the peak with blue (resp. yellow) text. The model parameters have been specified in the main text.

## II. ADDITIONAL ANALYSIS OF $\text{CaP}_3$

We derive in Sec. II A the effective-mass model that was used in the main text. Sec. II B provides more details on the calculation of Landau levels.

Throughout this section, we use  $\text{\AA}$  as the length unit and eV as the energy unit. We also neglect the spin-orbit interaction, whose energy scale is predicted to be in the range 4 to 30 meV<sup>10</sup>. This energy scale is comparable to the Landau-level spacing (presented below) at fields between 5 T and 10 T, therefore our numerical simulations should not be viewed as a quantitative model of the magnetic energy levels of  $\text{CaP}_3$ ; rather, they should be viewed as proof of principle for the existence of Landau-Dirac points in  $\text{CaP}_3$ . (We remind the reader that Landau-Dirac points are perturbatively robust to spatial-inversion-symmetric perturbations – including the spin-orbit interaction.) A quantitative model of magnetized  $\text{CaP}_3$  must account for the Zeeman interaction and a realistic spin-orbit interaction – a project we leave to future investigations.

### A. Effective-mass model of $\text{CaP}_3$

The effective-mass model of  $\text{CaP}_3$  around the Y point can be found in Ref. [10]. The spinless Hamiltonian is written as

$$\begin{aligned}
 H(\mathbf{k}) &= \sum_{i=0}^3 g_i \sigma_i \\
 g_0 &= a_0 + a_1 k_a^2 + a_2 k_b^2 + a_3 k_c^2, \\
 g_1 &= 0, \\
 g_2 &= \alpha k_a + \beta k_b + \gamma k_c, \\
 g_3 &= m_0 + m_1 k_a^2 + m_2 k_b^2 + m_3 k_c^2, \\
 a_0 &= -0.091, a_1 = 1.671, a_2 = 14.372, a_3 = 2.394, \\
 m_0 &= -0.142, m_1 = 10.438, m_2 = 19.138, m_3 = 11.91, \\
 \alpha &= 1.773, \beta = 0.001, \gamma = -2.096.
 \end{aligned} \tag{8}$$

Here,  $\sigma_{1,2,3}$  are Pauli matrices,  $\sigma_0$  is the two-by-two identity matrix,  $k_a$ ,  $k_b$  and  $k_c$  are reduced coordinates corresponding to the reciprocal-lattice vector of  $\text{CaP}_3$ . Using Cartesian coordinates, the parameters  $g_i$  becomes:

$$\begin{aligned}
 g_0 &= -0.091 + 5.348k_x^2 - 2.91k_x k_y + 49.303k_y^2 - 1.136k_x k_z - 31.67k_y k_z + 13.83k_z^2, \\
 g_2 &= 3.172k_x - 0.8611k_y - 4.297k_z, \\
 g_3 &= 33.40k_x^2 - 18.18k_x k_y - 7.098k_x k_z + 67.6k_y^2 - 40.65k_y k_z + 49.83k_z^2 - 0.142.
 \end{aligned} \tag{9}$$

To simplify the Hamiltonian, we perform a series of transformations:

- We rotate the system such that  $g_2(\mathbf{k})$  only depends on  $k_z$ :

$$(k_x, k_y, k_z) = (k'_x, k'_y, k'_z) \begin{pmatrix} -0.7665 & 0.2081 & -0.6076 \\ 0.262 & 0.9651 & 0 \\ 0.5863 & -0.159 & -0.7943 \end{pmatrix}. \tag{10}$$

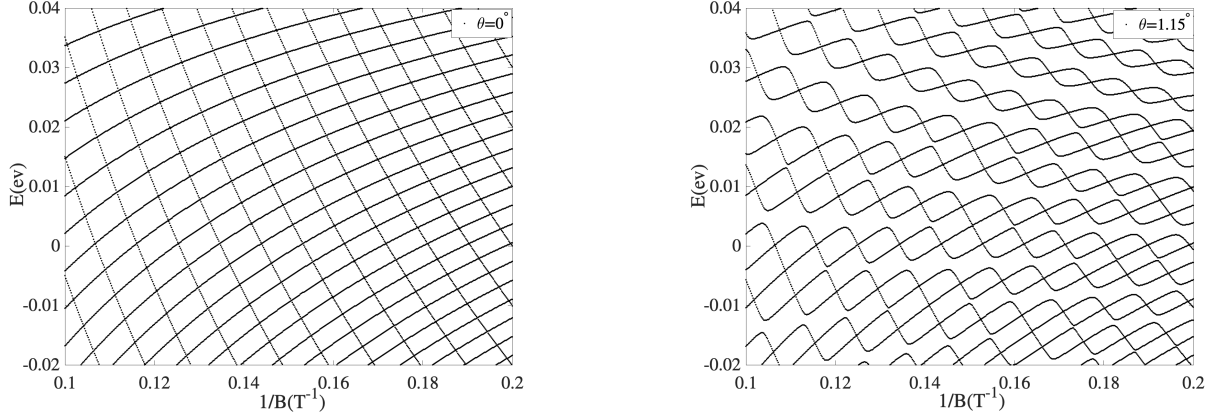


FIG. 2. Landau levels in the  $k_z = 0$  plane (field-fixed coordinates) for two field orientations.

- We perform a unitary transformation with  $U = (1 + i\sigma_z)/\sqrt{2}$  such that  $\sigma_x \rightarrow -\sigma_y$ ,  $\sigma_y \rightarrow \sigma_x$ .
- We remove the  $k_x k_y$  term in  $g_0$  by defining

$$\begin{pmatrix} k''_x \\ k''_y \end{pmatrix} = \begin{pmatrix} 0.4295 & 0.90305 \\ -0.90306 & 0.4295 \end{pmatrix} \begin{pmatrix} k'_x \\ k'_y \end{pmatrix}, \quad k''_z = k'_z. \quad (11)$$

- We shift the energy  $g_0 \rightarrow g_0 + \mu_0 = g_0 + 0.01741$  such that the hole and electron pockets enclose the same volume at zero energy.

After all the above transformations, we obtain

$$\begin{aligned} g_0 &= 54.68k''_x{}^2 + 11.33k''_x k''_z + 5.188k''_y{}^2 - 1.75k''_y k''_z + 8.608k''_z{}^2 - 0.091, \\ g_1 &= 5.409k''_z, \\ g_3 &= 77.73k''_x{}^2 - 20.66k''_x k''_y + 15.74k''_x k''_z + 28.6k''_y{}^2 - 3.75k''_y k''_z + 44.49k''_z{}^2 - 0.142. \end{aligned} \quad (12)$$

These coefficients of the transformed Hamiltonian  $H(\mathbf{k}'') = \sum_{i=0}^3 g_i \sigma_i$  will be used in the subsequent calculation of Landau levels. The convenience attained with this coordinate system is that  $g_1$  vanishes within the ( $k''_z = 0$ ) plane, so that the two-by-two Hamiltonian is diagonal with diagonal elements  $H_{11}$  and  $H_{22}$ ; we thus refer to these coordinates as the *diagonal coordinate system*, and henceforth drop the primes on  $k_x$ ,  $k_y$  and  $k_z$ .

It is convenient to remove the  $k_x k_y$  term in  $H_{11}$  by

$$\begin{pmatrix} k'_x \\ k'_y \end{pmatrix} = \begin{pmatrix} -0.9947 & 0.103 \\ -0.103 & -0.9947 \end{pmatrix} \begin{pmatrix} k_x \\ k_y \end{pmatrix}, \quad (13)$$

and the  $k_x k_y$  term in  $H_{22}$  by

$$\begin{pmatrix} k''_x \\ k''_y \end{pmatrix} = \begin{pmatrix} -0.7 & 0.7133 \\ -0.7133 & -0.7 \end{pmatrix} \begin{pmatrix} k_x \\ k_y \end{pmatrix}, \quad (14)$$

giving finally  $H_{11} = -0.2156 + 133.485k''_x{}^2 + 32.7191k''_y{}^2$ ,  $H_{22} = 0.06841 - 33.56k''_x{}^2 - 12.9k''_y{}^2$ .

## B. Landau levels of CaP<sub>3</sub>

We have performed calculations for various orientations of the magnetic field, relative to a fixed crystallographic axis. For each orientation, we always adopt a right-handed Euclidean coordinate system such that the magnetic field lies in the  $-z$  direction; such a system is uniquely defined up to rotations about the  $z$  axis, and will be referred to as *field-fixed coordinates*. No matter the field orientation, every  $\mathbf{k}$  point in the  $k_z = 0$  plane (in field-fixed coordinates) is mapped to itself by spatial-inversion symmetry.

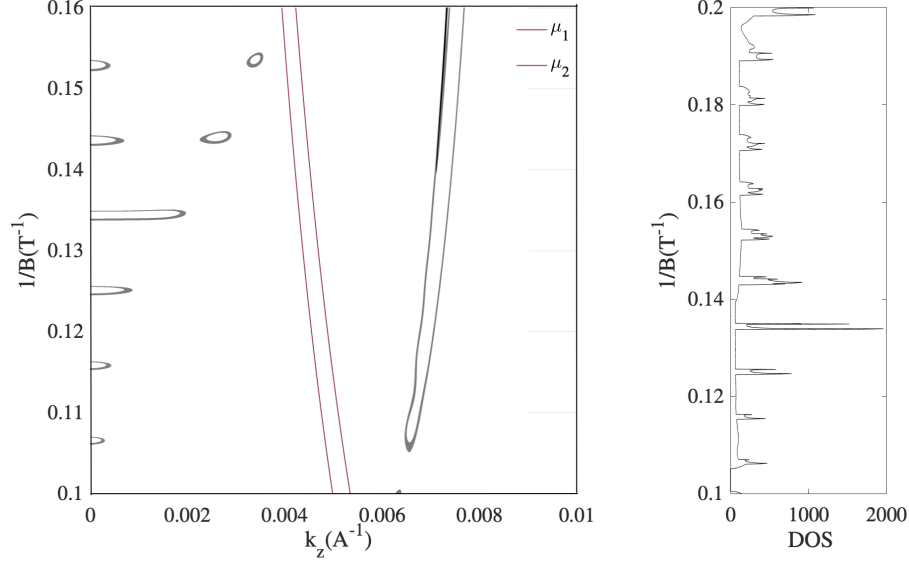


FIG. 3. For the spinless model of  $\text{CaP}_3$ , we plot the Landau-Fermi surface over  $(1/B, k_z)$ -space in panel (a), and the corresponding density of states in panel (b).

Generally, the field-fixed coordinates differ from the diagonal coordinates defined in Sec. II A. When both coordinate systems coincide, the magnetic energy levels (in the  $k_z = 0$  plane) are obtained from separately diagonalizing the Peierls-Onsager Hamiltonians  $H_{11}(\mathbf{K})$  and  $H_{22}(\mathbf{K})$ . These are obtained from  $H_{11}(\mathbf{k})$  and  $H_{22}(\mathbf{k})$  (defined in the previous subsection) by the standard Peierls substitution:  $(k_x, k_y) \rightarrow (k_x + By, k_y)$ , in the Landau electromagnetic gauge  $\mathbf{A} = (By, 0, 0)$ , with  $[y, k_y] = i$ . (Note that the principal coordinate axes for  $H_{11}(\mathbf{k})$  and  $H_{22}(\mathbf{k})$  are distinct, so the above Peierls substitutions are really carried out in different coordinate systems; this subtlety will affect neither the energy levels nor our conclusions about symmetry-protected crossings.) For either Hamiltonian, the Landau-level wave functions are labelled by  $n \in 0, 1, 2 \dots$  and wavenumber  $k_x$ , and have the analytic form:  $\psi_{nk_x} = \exp(ik_x x) H_n(\alpha y)$ , where  $\alpha$  is a constant and  $H_n$  is the Hermite polynomial<sup>11</sup>. The corresponding magnetic energy levels are presented in Fig. 2(a).

The following symmetry analysis is useful to determine the stability of the Landau-Dirac crossings. The inversion symmetry acts on eigenstates  $\{\psi_{nk_x}\}_{n, k_x}$  of  $H_{11}(\mathbf{K})$  as  $\hat{i}\psi_{nk_x}(y) = (-1)^n \psi_{n, -k_x}(y)$ , where  $(-1)^n$  originates from inverting the Hermite function. It is convenient to map  $-k_x$  back to  $k_x$  by the magnetic translation:

$$\hat{t}(\mathbf{R}) = e^{-i[\hat{p} + \mathbf{A}(r) - \mathbf{B} \times r] \cdot \mathbf{R}} \quad (15)$$

which is also a symmetry of the Peierls-Onsager Hamiltonian<sup>12,13</sup>. In particular,  $\hat{t}(2k_x \hat{y}/B) \psi_{n-k_x}(y) = \psi_{nk_x}(y)$ , with  $\hat{y}$  the unit vector in the  $y$  direction. Therefore, we deduce

$$\hat{i}\hat{t}(2k_x \hat{y}/B) \psi_{nk_x}(y) = (-1)^n \psi_{nk_x}(y), \quad (16)$$

which states that adjacent Landau levels [for  $H_{11}(\mathbf{K})$ ] belong to opposite eigenspaces of the operator  $\hat{i}\hat{t}(2k_x \hat{y}/B)$ . Based on this symmetry analysis, and the analogous analysis for  $H_{22}(\mathbf{K})$ , we demonstrated in the main text that half the Landau-Dirac crossings in Fig. 2(a) are crossings between states in different  $\hat{i}\hat{t}(2k_x \hat{y}/B)$  representations; the other half are protected by a different symmetry which exists only when the field-fixed and diagonal coordinates coincide.

Thus one expects that half the Landau-Dirac crossings in Fig. 2(a) destabilize upon tilting of the field. This is confirmed by a calculation for which the field is tilted in the  $x - z$  plane (diagonal coordinates) by an angle  $\theta = 1.15^\circ$  relative to the  $-z$  axis (diagonal coordinates); the resultant Landau levels in the  $k_z = 0$  plane (field-fixed coordinates) are shown in Fig. 2(b). For this calculation, analytic solutions are not available and thus numerical diagonalization is performed by standard techniques<sup>14</sup>.

Finally, we show in Fig. 3(a) the Landau-Fermi surfaces of the magnetic energy levels at zero energy (the charge-neutral point); this plot is an expanded version of Fig. 3(b) in the main text. The type-I Landau-Fermi surfaces result in batman peaks in the density of states, as illustrated in the right panel.

Observe that the type-I Landau-Fermi surfaces are confined (roughly) to the left half of the plot, where quantum tunneling is non-negligible. To make this observation precise, we calculate the Landau-Zener parameter  $\mu(B^{-1}, k_z)$  for each of the four breakdown regions in the graph of  $\text{CaP}_3$ .  $\mu$  is calculated by linearizing the effective-mass Hamiltonian at each of the four sausage links, then computing  $\mu = S_{\square}/8B$  (with  $S_{\square}$  the area of the  $\mathbf{k}$ -rectangle inscribed by the hyperbolic band contours), just as we did for our two-pocket model in the main text. Accounting for  $\hat{i}$  symmetry, there are two (instead of four) independent

values of  $\mu$ , given by  $\mu_1=5.571 \times 10^4 k_z^2/B$  and  $\mu_2=6.4 \times 10^4 k_z^2/B$ .  $\mu_1=\mu_2=1/\pi$  defines two curves in  $(B^{-1}, k_z)$ -space colored red in Fig. 3(a). To the right of both curves, the tunneling probability  $P_{1,2} = e^{-2\pi\mu_{1,2}} < e^{-2}$  is negligible, and the Landau-Fermi surface is determined by four independent cyclotron orbits over the four pockets.

- 
- <sup>1</sup> L. Onsager, “Interpretation of the de Haas-van Alphen effect,” *Philos. Mag.* **43**, 1006–1008 (1952).
- <sup>2</sup> L. M. Lifshitz and A.M. Kosevich, “Theory of magnetic susceptibility in metals at low temperatures,” *J. Exp. Theor. Phys.* **2**, 636 (1956).
- <sup>3</sup> Joseph B. Keller, “Corrected Bohr-Sommerfeld quantum conditions for nonseparable systems,” *Ann. Phys. (N. Y.)* **4**, 180 – 188 (1958).
- <sup>4</sup> Laura M. Roth, “Semiclassical theory of magnetic energy levels and magnetic susceptibility of Bloch electrons,” *Phys. Rev.* **145**, 434–448 (1966).
- <sup>5</sup> G. P. Mikitik and Yu. V. Sharlai, “Manifestation of Berry’s phase in metal physics,” *Phys. Rev. Lett.* **82**, 2147–2150 (1999).
- <sup>6</sup> A. Alexandradinata and Leonid Glazman, “Semiclassical theory of Landau levels and magnetic breakdown in topological metals,” *Phys. Rev. B* **97**, 144422 (2018).
- <sup>7</sup> Clarence Zener and Ralph Howard Fowler, “Non-adiabatic crossing of energy levels,” *Proc. R. Soc. Lond. A* **137**, 696–702 (1932).
- <sup>8</sup> M.I. Kaganov and A.A. Slutskin, “Coherent magnetic breakdown,” *Phys. Rep.* **98**, 189 – 271 (1983).
- <sup>9</sup> L. M. Falicov and Henryk Stachowiak, “Theory of the de Haas-van Alphen effect in a system of coupled orbits. application to magnesium,” *Phys. Rev.* **147**, 505–515 (1966).
- <sup>10</sup> Qiunan Xu, Rui Yu, Zhong Fang, Xi Dai, and Hongming Weng, “Topological nodal line semimetals in the CaP<sub>3</sub> family of materials,” *Phys. Rev. B* **95**, 045136 (2017).
- <sup>11</sup> L. D. Landau and E. M. Lifshitz, *Quantum Mechanics* (Elsevier, Singapore, 2007).
- <sup>12</sup> J. Zak, “Magnetic translation group,” *Phys. Rev.* **134**, A1602–A1606 (1964).
- <sup>13</sup> E. Brown, “Bloch electrons in a uniform magnetic field,” *Phys. Rev.* **133**, A1038–A1044 (1964).
- <sup>14</sup> Chong Wang, Wenhui Duan, Leonid Glazman, and A. Alexandradinata, “Landau quantization of nearly degenerate bands and full symmetry classification of Landau level crossings,” *Phys. Rev. B* **100**, 014442 (2019).